Charge exchange (p,n) reactions to the isobaric analog states of high Z nuclei: $73 \leq Z \leq 92$

L. F. Hansen, S. M. Grimes,* C. H. Poppe, and C. Wong
University of California, Lawrence Livermore National Laboratory, Livermore, California 94550
(Received 14 January 1983; revised manuscript received 15 August 1983)

Differential cross sections have been measured for the (p,n) reaction to the isobaric analog states of ^{181}Ta, ^{197}Au, ^{209}Bi, ^{232}Th, and ^{238}U at an incident energy of 27 MeV. Because of the importance of collective effects in this mass region, coupled-channel calculations have been carried out in the analysis of the data. Optical potentials obtained from the Lane model for the charge exchange reaction have been used in the simultaneous analysis of coupled proton and neutron channels. The sensitivity of the calculations to the different couplings between the levels and to the magnitude of the isovector potentials, V_1 and W_1, is discussed. The good agreement obtained between the measured and calculated (p,n) angular distributions to the analog state confirms the validity of the Lane formalism for high-Z nuclei ($Z \geq 50$). Elastic neutron differential cross sections inferred from the coupled-channel analysis are compared with measurements available in the literature in the energy range 7—8 MeV. The results of these calculations agree with the measured values as well as the results of calculations made using global neutron optical potential parameters optimized to fit neutron data.

[NUCLEAR REACTIONS ^{181}Ta, ^{197}Au, ^{209}Bi, ^{232}Th, ^{238}U(p,n)IAS; $E=27$ MeV; Measured $\sigma(\theta)$ for ground-state analog transition; deduced (n,n)$\sigma(\theta)$, $E=7-8$ MeV; coupled-channel analysis.]

INTRODUCTION

The optical model formalism and the isotopic spin dependence introduced by Lane[1] in the optical model potential (OMP) have successfully described quasielastic (p,n) reactions to the isobaric analog state (IAS) of the target ground state (g.s.) for medium mass[2-4] and light nuclei.[5,6] Furthermore, Lane's reformulation of the OMP from the charge-independent two-body force, has allowed elastic neutron scattering cross sections to be calculated with neutron potentials extracted from proton data: (p,p) and $(p,n)_{IAS}$. These calculations have been shown[2-4] to be in fairly good agreement with elastic neutron measurements reported for $Z \geq 50$ nuclei.[7-9] Schery *et al.*[10] extended this analysis to (p,n) measurements in heavier nuclei, $79 \leq Z \leq 90$. They carried out distorted-wave Born approximation (DWBA) calculations for the quasielastic differential cross sections and were moderately successful in fitting the data; however, the neutron elastic differential cross sections calculated with the OMP obtained from their analysis were in poor agreement with the measured cross sections.[7-9] It was not possible to conclude from their results if this marginal agreement was the result of their DWBA analysis and/or of limitations of the Lane model when applied to high-Z nuclei, especially when these nuclei have static deformations.

In order to test further the validity of the Lane model for heavy nuclei, we have measured the $(p,n)_{IAS}$ cross sections for ^{181}Ta, ^{197}Au, ^{209}Bi, ^{232}Th, and ^{238}U at an incident proton energy of 27 MeV. The $(p,n)_{IAS}$ cross sections for Th and U were also measured at 26 MeV because of existing elastic proton measurements[11] at this energy. The (p,p) and $(p,n)_{IAS}$ differential cross sections were calculated by solving the Lane coupled-channel (CC) equations for the proton and neutron channels. Because of the intrinsic width[12,13] of the analog state for the nuclei studied in the present work, $\Delta E_{IAS} \simeq 150-250$ keV, inelastic analog levels with separation energies ≤ 250 keV from the analog state cannot be resolved from the g.s. analog. Consequently, in order to compare the calculations with the measurements, not only must the g.s. transition be calculated, but the transitions to the unresolved inelastic analog levels must also be included. The need to calculate these excited-state-analog cross sections (together with the strong collective nature of some of the target nuclei, as it is the case for the Ta, Th, and U targets which are characterized by large and permanently deformed mass and charge distributions),[14,15] made it necessary to carry out CC calculations for the inelastic proton and neutron channels. The vibrational nuclei Au and Bi are also characterized by collective effects,[16-19] and although they are less important in the calculation of the g.s. transition, in all the analyses presented here, the Lane equations were generalized to include couplings to the low excited states of the target and their analogs.

We obtained good agreement between the measured neutron elastic differential cross sections[7-9] at 7—8 MeV and the predicted neutron cross sections calculated using the neutron potentials obtained from the present analysis. This agreement supports the validity of the Lane model, even for very heavy nuclei where large isospin mixing in the decay channel is expected and where coupled-channel and deformation effects must be considered in the charge exchange (p,n) reaction. We show that the quality of the

agreement between the calculations presented here and the measurements is determined by the completeness of the calculations and that DWBA calculations are not appropriate to regions of strong collectivity. The calculated elastic neutron cross sections agree with experiment as well as the results of calculations obtained using global parameters[20,21] optimized to fit neutron data.

EXPERIMENTAL METHOD AND DATA REDUCTION

The cross section measurements were made using the maximum energy proton beam (27 MeV) from the Lawrence Livermore National Laboratory (LLNL) cyclograaff accelerator. (The Th and U measurements were also made at 26 MeV.) Emitted neutrons were detected using the LLNL time-of-flight (TOF) facility,[22] where sixteen NE-213 scintillator detectors (11.4 cm diameter by 5.1 cm long) cover the angular region from 3° to 159°, allowing a neutron angular distribution between these angles to be measured simultaneously. The flight path was 10.75 m for each detector, and pulse shape discrimination was used to reduce the gamma-ray background. A more detailed discussion of the experimental techniques and detector efficiency is found in Ref. 22(b).

The Ta, Au, and Bi targets were self-supporting 2.54-cm-diam foils of areal density 4.0, 2.7, and 5.3 mg/cm^2, respectively; the Th and U targets, also self-supporting foils, were 1.27 cm in diameter and about 5 mg/cm^2 thick. A second set of thicker Th and U foils ($\sim$15 mg/cm^2) was also used; reasons for using this second set are discussed below.

To prevent the overlap of the high-energy neutrons from a given burst with low-energy neutrons coming from previous bursts, the detectors were biased at 3.5 MeV. The energy of the neutrons that leave the residual nucleus in the analog of the g.s. of the above targets varies between 6.5 MeV for U to about 9 MeV for Ta. In addition, the 25-MHz cyclotron beam was swept before injection into the tandem in order to reduce the beam burst rate on target to 5 MHz.

The integration of the peak areas corresponding to the analog states (IAS) in these heavy nuclei required special attention. For (p,n) reactions on lighter targets ($A \leq 150$), the natural width of the IAS is sufficiently small so that the observed width results almost entirely from proton energy loss in the target, time width of the incident beam, and time resolution of the detectors and electronics. It is therefore reasonable to assume that the shape of the peak is Gaussian, because it is the result of a number of independent contributions. For nuclei with $A \simeq 200$, the IAS widths are about 200 keV (Refs. 12 and 13); when experimental circumstances are such that the natural linewidth dominates, the peak should be described by a Breit-Wigner shape, as pointed out by Galonsky *et al.*[23]

Our initial efforts to measure the cross sections were directed at obtaining very good experimental energy resolution so as to maximize the ratio of signal to background. For the targets with thicknesses of about 5 mg/cm^2, the proton energy loss was $\sim$50 keV. Because the time resolution tended to deteriorate during a long run, a series of short runs was made with optimum beam width ($\sim$1 ns) during each run. As a result, the statistical errors characterizing the data in each run were large. We could obtain fits with either a Gaussian or a Breit-Wigner shape having reasonable χ^2, but the peak areas inferred from the two fits differed by about 35%. Furthermore, it was not possible to make a visual choice between the two functions because the actual shape was intermediate between the two types of fits. To overcome this problem, the measurements were repeated with a proton beam tuned for maximum current rather than minimum time width, and the running times were extended over much longer periods to further improve the statistical accuracy at the expense of an additional time broadening. These measurements have a typical time resolution of about 2.5 ns. For the lighter targets, Ta,Au,Bi, this broadening of the peaks was sufficient to obtain reasonable fits with a Gaussian shape and rule out the fits with the Breit-Wigner form on the basis of the χ^2 values obtained (see Fig. 1). For the Th and U measurements, in addition to the broadening of the peaks as described above, thicker targets ($\sim$15 mg/cm^2) were used, which increased the proton energy loss to about 130 keV and the peak widths to about 300 keV. These wider peaks were also well fitted by a Gaussian form.

The errors in the extracted peak areas were estimated to

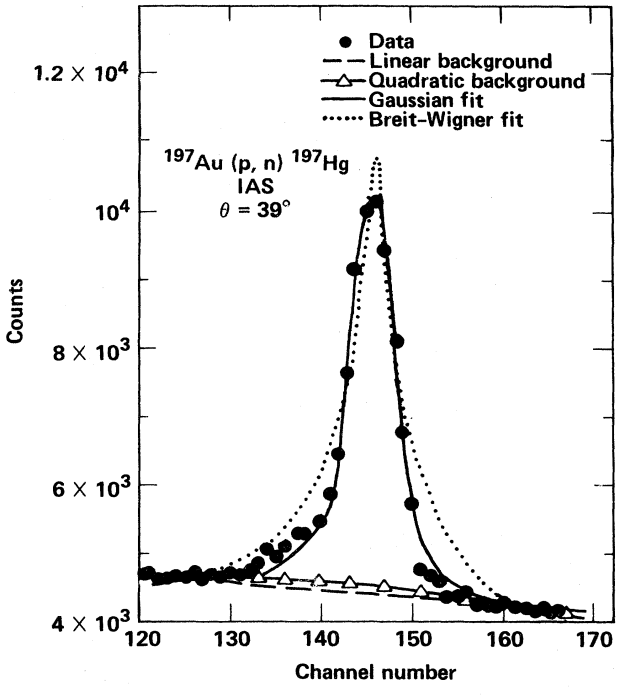

FIG. 1. Neutron spectrum from the ^{197}Au(p,n)^{197}Hg reaction at $\theta = 39°$ near the analog state. Data are indicated with closed circles. Backgrounds corresponding to best-fit linear and quadratic assumed forms are shown with dashed and Δ dashes, respectively. These correspond to the Gaussian fit. The Gaussian fit is shown with a solid line and the Breit-Wigner fit with a dotted one. Background for the Breit-Wigner fit is not shown but is lower than that for the Gaussian fit.

be less than 10% at forward angles, but remained large (30—35 %) for spectra at angles beyond 90°. It is not obvious how this situation can be improved, since the (p,2n) and (p,3n) reaction channels for all the targets and the fission reaction channel for Th and U lead to large neutron continua under the analog peaks, and the analog cross sections are very small in some angular ranges. The background subtraction for neutrons coming from the different reaction channels was assumed to have a linear shape in the TOF spectra under the IAS peak.

Recent investigations of the (p,n) reaction at energies above 100 MeV have found evidence[24,25] for a giant Gamow-Teller state at excitation energies $\Delta L=0, \Delta S=1$ transition, so it would be expected to have an angular distribution similar to that of the analog.

There are two reasons why we do not believe that possible Gamow-Teller (GT) state contributions influence our results. The investigation of Taddeucci *et al.*[24] suggests that the strength of the Gamow-Teller state relative to the isobaric analog state (Fermi state) decreases at low bombarding energy. Further, the GT state has a width which is about 4 MeV in this mass region.[25] This is sufficiently large relative to the experimental width of the analog states that the influence of such states would correspond to a slightly nonlinear background. In Fig. 1 we show a typical neutron spectrum in the vicinity of the analog state. The spectrum shown is for ^{197}Au(p,n)^{197}Hg at 39°. Two backgrounds are shown. The dashed line represents a best-fit linear background and the triangle-dashed line a best-fit quadratic background. This latter background is approximately that which would be produced by a GT state of width 4 MeV and strength comparable to the analog state. This change in background causes a change of only 6% in the area of the peak. The χ^2 values for the two fits with different backgrounds are very similar in nearly all cases and do not provide compelling evidence for the superiority of quadratic backgrounds. The integrals used in evaluating the cross sections were the ones obtained with the Gaussian fit and with best-fit linear[26] backgrounds. Given the small differences between the linear and quadratic fits, it appears unlikely that the GT state contributions could influence our cross sections beyond the uncertainties ascribed to fitting and statistical errors.

CALCULATIONAL ANALYSIS

The charge-exchange (p,n) reaction to the IAS of the target g.s. is described[1] in terms of the nondiagonal isospin matrix elements of the Lane potential

$$4(\vec{t}\cdot\vec{T})U_1(E,r)/A \ , \tag{1}$$

where $\vec{t}$ and $\vec{T}$ are the isospin operators for the incoming nucleon and the target nucleus, respectively; $U_1(E,r)$ is the isovector potential and is complex and independent of isospin, and A is the target mass number. The isovector potential also connects proton elastic scattering from the target nucleus A with neutron scattering from the isobaric analog state in the final nucleus B through the quasielastic $(\mathrm{p,n})_{\mathrm{IAS}}$ cross section, $\mathrm{p}+A(Z,N)\rightarrow B(Z+1,N-1)+\mathrm{n}$. The neutron leaves the residual nucleus, B, in the isobaric analog state of the target ground state and is emitted with an energy $E_\mathrm{n}=E_\mathrm{p}-\Delta_C$. The Coulomb displacement energy, Δ_C, between these two states is well approximated by the experimental relation,[27] $\Delta_C=1.444Z/A^{1/3}-1.13$ MeV, with $Z=\frac{1}{2}(Z_A+Z_B)=Z_A+\frac{1}{2}$. For the present targets, the value of Δ_C is about 20 MeV.

Introducing the Lane potential into the nuclear part of the optical model potential (OMP), one obtains

$$U_N(E,r)=U_0(E,r)+4(\vec{t}\cdot\vec{T})A^{-1}U_1(E,r) \ , \tag{2}$$

where U_0 and U_1 are complex and are the isoscalar and isovector parts of the nuclear potential, respectively. The potential for the protons scattered from the target A at an energy E_p is given by

$$U_{\mathrm{p}A}(E_\mathrm{p})=U_0-\frac{T_0U_1}{2A}=U_0-\xi U_1 \ . \tag{3}$$

T_0 corresponds to the minimum value of T for the target and is equal to its component T_3, $T_0=T_3=(N-Z)/2=\xi A/2$, where ξ is the symmetry parameter found in most of the global OMP. Similarly, the potential for neutrons scattered from the analog level in the final nucleus B at an energy $E_\mathrm{n}=E_\mathrm{p}-\Delta_C$ is given by

$$U_{\mathrm{n}B}(E_\mathrm{n})=U_0+\frac{T_0-1}{2A}U_1=U_0+(\xi-2/A)U_1 \ . \tag{4}$$

The Lane equation connects the potential for the system (nB) with the potential for neutrons scattered elastically from the target (nA) at energy E_n. The OMP for neutrons elastically scattered from target A at E_n differ[1] only from the above proton potentials [Eq. (3)] in the sign of the symmetry term,

$$U_{\mathrm{n}A}(E_\mathrm{n})=U_0+\frac{T_0U_1}{2A}=U_0+\xi U_1 \ . \tag{5}$$

For heavy nuclei studied here, the difference between the neutron potentials given by Eqs. (4) and (5) is small (1—6 %). The neutron OMP extracted from the present calculations correspond to neutron energies $E_{\mathrm{n}B}=(27\ \mathrm{MeV}-\Delta_C)$, ranging from 6.5 (^{238}U) to 9.3 MeV (^{181}Ta) because of the large value of the Coulomb displacement energy for these nuclei ($\Delta_C\simeq 20$ MeV).

The Coulomb field reduces the energy of the incident proton, and, because of the energy dependence of the phenomenological OMP, the incident proton sees an effective nuclear potential corresponding to a lower energy. A Coulomb correction term, $\Delta U_C(E,r)$, also assumed to be complex,[28] has been introduced explicitly in the nuclear potential. The radial average of the correction to the real depth $\langle\Delta V_C(E,r)\rangle_r$ has been estimated by Satchler[29] to equal $0.4Z/A^{1/3}$ assuming that the isoscalar potential $V_0(E)$ has a linear dependence on energy of the type $V_0(E)=V(0)-\alpha E$, with $\alpha=0.3\ \mathrm{MeV}^{-1}$ and the Coulomb radius parameter $r_C=1.3$ fm. The magnitude of this correction calculated in the form just described is known as a "full" Coulomb correction. The imaginary term, $\Delta W_C(E,r)$, is not well understood, since its calculation may be complicated by the strong energy dependence of the radial shape of the absorption potential: $W(E,r)$ goes from a surface imaginary potential to a volume potential

as the energy increases. Rapaport[30] has obtained an empirical energy dependence for ΔW_C, assuming a surface radial dependence, $\Delta W_C(E)=(-0.5Z/A^{1/3})(1-0.028E)$. In the present analysis, however, the Coulomb corrections only enter when the proton potential adjusted to fit the $(p,n)_{IAS}$ data is converted to a neutron potential. In the two global sets[31,32] of proton optical model (OM) parameters used in the present calculations, the Coulomb correction term is only present in the expression of the real potential V (see Table I). The neutron potentials used in the calculations of the neutrons emitted from the analog state (nB), and those elastically scattered from the target nuclei (nA), were calculated according to Eqs. (4) and (5), respectively. The procedure we adopted was to drop the Coulomb correction term given in the parametrization of the adjusted proton potential[31,32] and to evaluate Eqs. (4) and (5) at the appropriate neutron energy $(E_p-\Delta_C)$ using the energy dependence of the parametrizations. As described below, the proton potential isovector strengths were readjusted to fit the $(p,n)_{IAS}$ data, and the proton isoscalar strengths were suitably modified so as to conserve the total real and imaginary proton potential strengths.

Of the nuclei studied in this paper, ^{181}Ta, ^{232}Th, and ^{238}U are rotational nuclei characterized by large static deformations.[15,16] These deformations give rise to collective motions that result in strong couplings between the low-lying excited states and the ground state and between different excited levels. Similarly, the vibrational nuclei, ^{197}Au and ^{209}Bi, show in their level structure significant collective effects.[16–19] An accurate calculation of the scattering from these nuclei and of the quasielastic $(p,n)_{IAS}$ reaction must include the coupling to the collective inelastic channels. Similarly, in the $(p,n)_{IAS}$ reaction, to account properly for excitation of excited analogs and their effect on the ground-state (p,n) transition, multistep processes must be included. They are important because of the strength of the coupling—both inelastic and charge exchange—and because the multistep contributions to the scattering amplitude are in phase with each other and are large, relative to the one-step direct process. Madsen and Brown[33] have shown the importance of multistep processes in the calculation of the $(p,n)_{IAS}$ cross sections. A very successful calculational approach to account for these collective effects in the description of the $(p,n)_{IAS}$, the proton, or the neutron scattering differential cross sections, is the coupled-channel (CC) method[14] using Tamura's formalism,[34] which permits an exact solution of the Lane coupled-channel equations.

The coupled-channel code of Stomp *et al.*[35] was used to perform exact Lane CC calculations for the $(p,n)_{IAS}$ and proton elastic differential cross sections; inelastic scattering to low-lying excited states and charge exchange to their analogs were also included to account for collective effects. Because of differences in the collective nature of the target nuclei and differences in their nuclear structure, the description of the CC calculations is different for each target, with the exception of Th and U. These nuclei, which are described first, are both characterized as rotors with $K=0$ ground-state bands. Furthermore, for Th and U, $(p,n)_{IAS}$ measurements were also performed at 26 MeV because of the existence of proton scattering data at that energy.[11]

^{232}Th$(p,n)_{IAS}$ ^{232}Pa AND ^{238}U$(p,n)_{IAS}$ ^{238}Np

The CC calculations were carried out using a collective OMP to account for the nuclear deformations. The deformed OMP were generated by replacing the real, imaginary, and Coulomb radii by

$$R(\theta)=r_0A^{1/3}[1+\Sigma_\lambda\beta_\lambda Y_{\lambda0}(\theta)]\,, \tag{6}$$

where the symbols have the standard definitions given in Ref. 31.

The levels and couplings included in these calculations are shown in Fig. 2. The 6^+ levels, with excitation energies 0.333 and 0.307 MeV in ^{232}Th and ^{238}U, respectively, were not included because the contribution to the measured $(p,n)_{IAS}$ cross sections resulting from couplings to these levels was negligible and did not justify the increase in computer time. Furthermore, the excitation energy of the 6^+ level (>300 keV) is larger, although marginally so, than the expected width[13,14] of about 250 keV for the ana-

TABLE I. Proton global optical model potentials.

Parameters	Menet *et al.*[a]	Becchetti-Greenlees[b]
V (MeV)	$49.9-0.22E+0.4Z/A^{1/3}+26.4\xi$	$54.0-0.32E+0.4Z/A^{1/3}+24\xi$
W_V (MeV)	$1.2+0.09E$	$0.22E-2.7$
W_D (MeV)	$4.2-0.05E+15.5\xi$	$11.8-0.25E+12.0\xi$
V_{SO} (MeV)	6.04	6.20
r_R[c]	1.16	1.17
a_R	0.75	0.75
r_i	1.37	1.32
a_i	$0.74-0.008E+1.0\xi$	$0.51+0.7\xi$
r_{SO}	1.064	1.01
a_{SO}	0.78	0.75
r_C	1.25	1.25

[a]Reference 31.
[b]Reference 32.
[c]All geometrical parameters in fm.

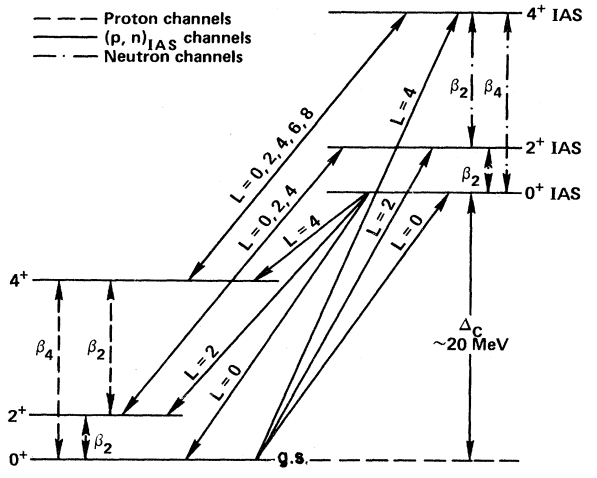

FIG. 2. Coupling scheme used in the CC calculations for the proton scattering and $(p,n)_{IAS}$ reactions from ^{232}Th and ^{238}U.

log state in this region. In principle, the neutrons from the 6^+ analog could have been resolved from the g.s. analog in the high-resolution measurements if the magnitude of the cross sections were significant compared to the ground-state IAS cross sections. However, no evidence for these states could be seen above background in any of the high-resolution spectra. The $(p,n)_{IAS}$ to the 2^+ and 4^+ levels must be included in the calculations because of the collective nature of the final nucleus and because of the fact that the measured IAS peak may include[12,13] transitions to these residual excited states.

The OM parameters for the CC calculation were taken from the global set of Menet *et al.*,[31] which reproduces the proton elastic and inelastic measurements[11] better than the Becchetti and Greenlees[32] (BG) parameters. Both OMP are given in Table I. The magnitude of the absorption potentials, W_V and W_D, used in the CC calculations were reduced by about 30% from the values given in the table to account for the couplings to excited states; with this reduction, the magnitude of the total reaction cross section was equal to that obtained in the spherical OM calculation of the elastic scattering. As discussed in Ref. 11, the correction to the absorption potential for the level with the maximum angular momentum, J_m, included in the CC calculation is smaller than the correction applied to the potential used for the g.s. and J_{m-2} levels by a factor, $\frac{3}{2}(J_m+1)(J_m+2)/(2J_m+1)(2J_m+3)$, in order to correct for the lack of couplings of the state J_m to higher states with $J \geq J_{m+2}$. For the 4^+ level, the highest angular momentum state included in the present calculations, the correction[11] to the absorption potential was 0.455 of 30%, equivalent to a reduction of only 14% of the values given in Table I.

Figure 2 shows the states in Th and U and their analogs that were included in the coupled-channels calculation. The direct couplings between states in the target and those in the residual nucleus are shown as solid arrows, and allowed values for transferred orbital angular momenta for these transitions are indicated. The inelastic transitions in the target and residual nucleus are depicted by the dashed and dot-dashed arrows, respectively, and the corresponding deformation parameters are shown. In the subsequent calculations, the effect of the multipolarity of the coupling between analog states (solid arrows) was investigated. However, for the inelastic transitions, all multipolarities allowed by conservation of angular momentum were always included. When only $L=0$ coupling was allowed between analog states, the solid curves of Fig. 3 are the calculation for the $0^+ \rightarrow 0^+$, $0^+ \rightarrow 2^+$, and $0^+ \rightarrow 4^+$(p,n) analog-state transitions. For this case, the direct $0^+ \rightarrow 2^+$ and $0^+ \rightarrow 4^+$ transitions are excluded and population of the excited analog states proceeds by multistep processes involving inelastic transitions in the target and residual nuclei. When the $L=2$ coupling is included, the dashed curve of Fig. 3 results, which shows that the effect of the direct $0^+ \rightarrow 2^+$ analog coupling is small but not entirely negligible for a detailed comparison of measured and calculated cross sections. Including the $L=4$ analog coupling produces negligible effects on the $0^+ \rightarrow 0^+$ and $0^+ \rightarrow 2^+$ analog transitions, as indicated in the figure.

Although the intrinsic width of the isobaric analog level of the g.s. does not allow a separate measurement of the cross sections to the different states shown in Fig. 3, the

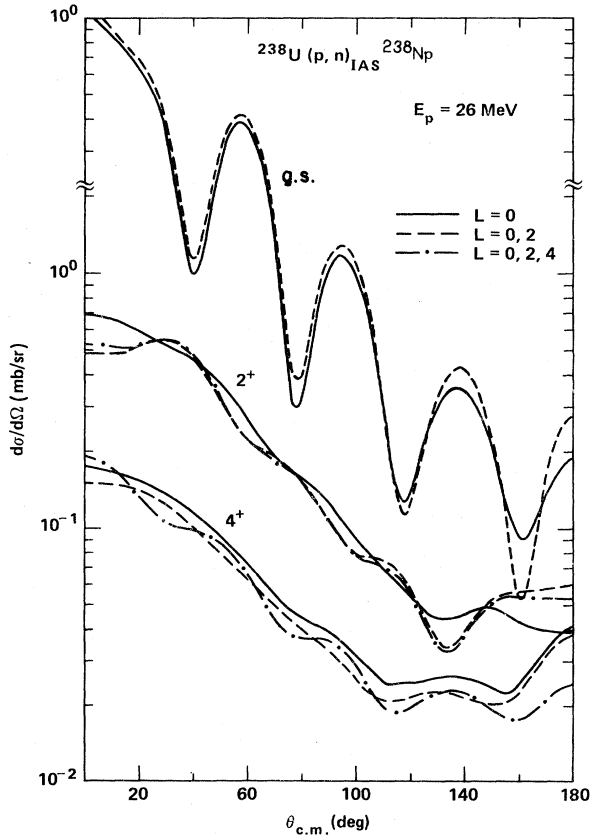

FIG. 3. Sensitivity of the $(p,n)_{IAS}$ differential cross sections to the multipolarity of the coupling between target states and analog states.

sum is still sensitive to the contribution of different multipolarities. Furthermore, it is important to notice (Fig. 3) that the calculated isobaric analog (IA) cross sections to the 2^+ level are comparable in magnitude to the g.s. IA cross sections; hence a meaningful comparison between measurements and calculations requires at least the inclusion of the 2^+ state in the CC calculations. The values of the deformation parameters, β_2 and β_4, used in the present calculations were 0.215 and 0.060 for ^{232}Th and 0.225 and 0.045 for ^{238}U, respectively.[11]

From the comparison of the calculated and measured (p,n) cross sections it became clear that the values of the real and imaginary strengths of the isovector potential, $V_1=26.4$ and $W_{D1}=15.5$ MeV (Table I) in the Menet *et al.* global set,[31] were too large. A reasonably good fit to the measured $(p,n)_{IAS}$ differential cross sections was obtained using $V_1=20$ and $W_{D1}=12$ MeV. The isoscalar potential strengths were corrected appropriately in order to maintain the prescribed[31] strengths of the real and surface imaginary potentials. Figure 4 shows the CC calculations with the above potentials, with proton and neutron potentials calculated according to the Lane formalism given by Eqs. (3) and (4), for the elastic and quasielastic proton differential cross sections at 26 MeV. The calculated $(p,n)_{IAS}$ curves represent the sum of the g.s., 2^+, and 4^+ calculated cross sections. The overall agreement with the measurements is quite good. To emphasize the importance of collective effects in this region of the Periodic Table, OM calculations for the proton elastic scattering with the OMP of Table I have also been plotted in Fig. 4. At angles $\theta \geq 60°$, the OM calculation overestimates the measured cross sections by 30% or more; a second OM calculation with the OMP of BG (Ref. 32) is also shown in Fig. 4; this calculation badly overestimates the cross sections at larger angles, producing larger discrepancies than those obtained for the previous calculation.[31]

The analysis of the $(p,n)_{IAS}$ differential cross-section measurements at 27 MeV proceeded in a similar way, although at this energy elastic measurements were not available. However, since both elastic and quasielastic reac-

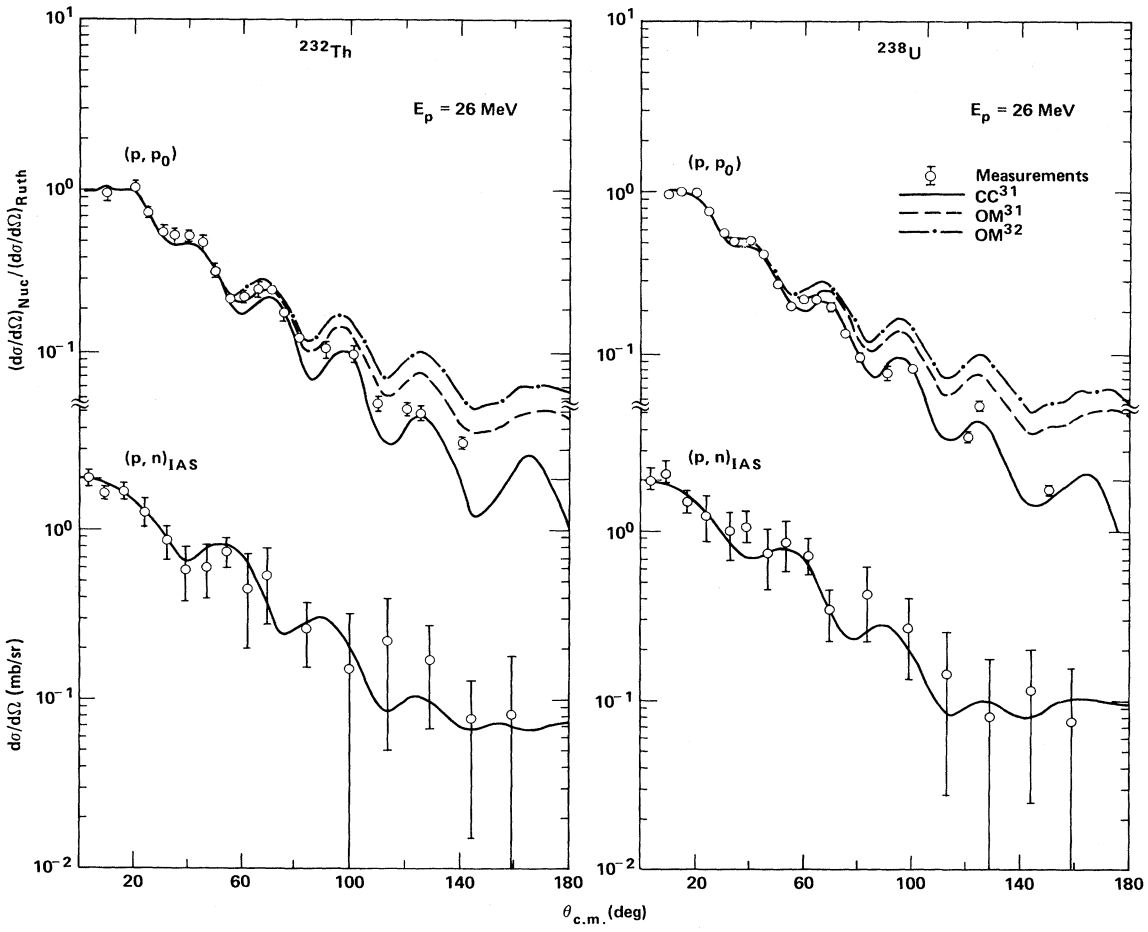

FIG. 4. CC fits to the measured elastic proton and $(p,n)_{IAS}$ differential cross sections for ^{232}Th and ^{238}U at 26 MeV using Lane-consistent OMP (Ref. 31) are shown by the solid curves. The CC calculations included in g.s., 2^+, and 4^+ states, and their analogs. OM calculations for the elastic proton scattering with OM parameters from Ref. 31 (dashed curves) and from Ref. 32 (dash-dotted curves) are also shown.

tions are the result of a direct interaction process, very small changes in the magnitude and shape of the differential cross sections are expected to occur for this small change in the incident proton energy. The closeness in shape and magnitude between the measured $(p,n)_{IAS}$ differential cross sections at 26 (Fig. 4) and 27 MeV (Fig. 5) corroborates this assumption. The main difference between these measurements is the smaller errors obtained for the latter, mainly at the larger angles. As was discussed earlier, the neutron peak corresponding to the analog states is superimposed on a large and steep background of fission neutrons, which decreases sharply with increasing neutron energy. An increase in energy of 1 MeV for the neutrons scattered from the analog state increases appreciably the ratio of analog neutrons to fission neutrons and improves the accuracy with which the $(p,n)_{IAS}$ cross sections could be extracted at 27 MeV relative to those obtained at 26 MeV. The CC calculations for the neutrons to the IAS using Menet *et al.*[31] OMP for the proton and the neutrons are shown in Fig. 5. The neutron potentials were calculated as already described for 26 MeV using the same values of the real and imaginary isovector potentials found at that energy. The complete set of all the OM parameters used in these calculations are listed in Table II. The measurements are compared with the calculations for the g.s. cross sections (upper curves), with the sum of g.s. and 2^+ cross sections and with the sum of g.s., 2^+, and 4^+ cross sections. The overall agreement of the sum of g.s., 2^+, and 4^+ cross sections (lower curves) with the data is quite good.

$^{181}Ta(p,n)_{IAS}\,^{181}W$

^{181}Ta has a rather large[14] quadrupole deformation with a deformation parameter $\beta_2 \simeq 0.260$. The low-lying level structure is characterized by collective rotational,[15] vibrational, and single-particle states.[14] The 137-keV ($\frac{9}{2}^+$) and 301-keV ($\frac{11}{2}^+$) levels are assumed to be members of the g.s. rotational band with $K=\frac{7}{2}$, while the 159-keV ($\frac{11}{2}^-$) level is a member of the $K=\frac{9}{2}$ rotational band built on the 6-keV ($\frac{9}{2}^-$) level.

The CC calculations carried out to describe the $(p,n)_{IAS}$ differential cross sections included the g.s., the 137-keV level, and their respective analogs in ^{181}W ($\Delta_C=-17.63$ MeV). The 301-keV level was not included because it is outside the range of the intrinsic energy width[12] of the analog level, 150—200 keV, characteristic of this mass region, $A=180$—200. The negative parity levels, $\frac{9}{2}^-$ and $\frac{11}{2}^-$, are not expected to contribute significantly to the analog cross sections and were not included in the CC calculations. Because of the absence of proton elastic scattering data from Ta near 27 MeV, the CC calculations were performed using the proton potentials of Menet *et al.*[31] and BG.[32] The neutron potentials for the (nB) channels were calculated as described earlier [Eq. (4)]. The magnitude of the isovector potential was obtained from the best fit to the $(p,n)_{IAS}$ data; the strengths of the real and imaginary isoscalar potentials, V_0 and W_0, were adjusted accordingly, in both proton and neutron potentials, in order to maintain the total strengths of V and W as prescribed

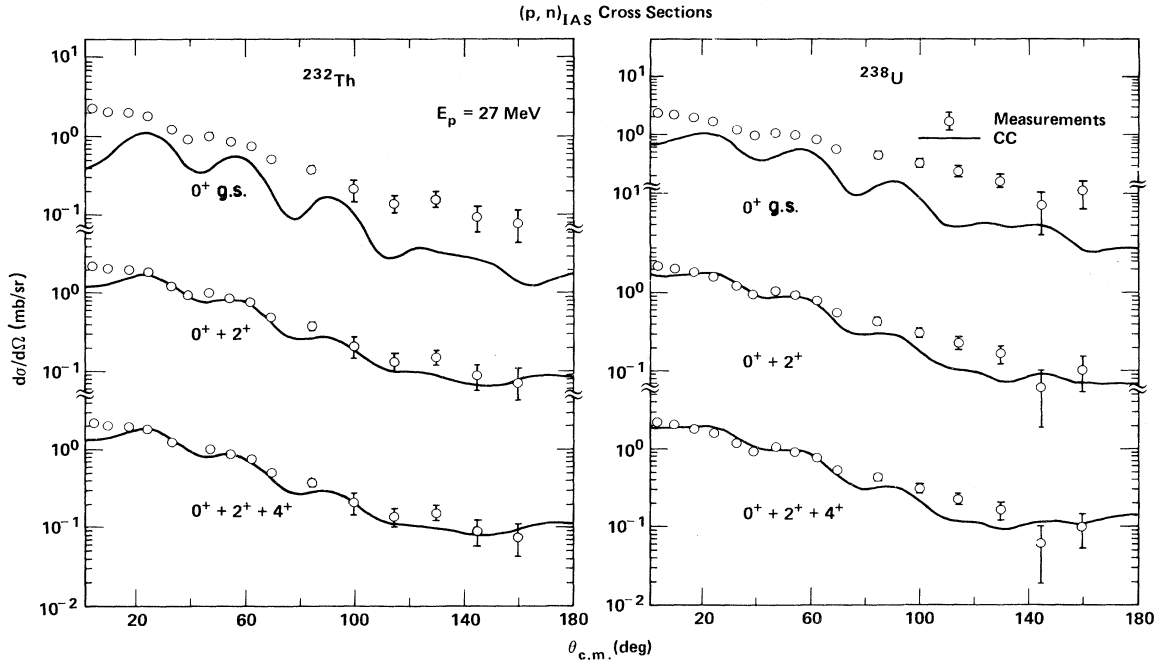

FIG. 5. Comparison of the measured $(p,n)_{IAS}$ differential cross sections for ^{232}Th and ^{238}U at 27 MeV with CC calculations using Lane-consistent OMP (Ref. 31): g.s. analog (upper curves); sum of the g.s. and excited 2^+ analogs (middle curves); sum of the g.s., excited 2^+, and 4^+ analog differential cross sections (lower curves).

TABLE II. Proton and neutron optical model potential strengths used in the CC calculations of the $(p,n)_{IAS}$ at 27 MeV and (n,n_0) measurements (Refs. 2–4).

Energy/OMP (MeV)	^{181}Ta	^{197}Au	^{209}Bi	^{232}Th	^{238}U
Δ_c	−17.63	−18.60	−19.20	−20.14	−20.42
$E(nB)$[a]	9.27	8.26	7.71	6.77	6.49
$E(nA)$[b]	8.05	8.05	8.05	7.00	7.00
Menet[c]					
V proton	54.23	54.62	54.99	55.74	55.89
W_v	3.63	3.63	3.63	3.63	3.63
W_D	5.85	5.92	6.04	6.32	6.37
$V(nB)$	47.33	47.15	46.80	45.54	45.11
W_v	2.03	1.94	1.89	1.81	1.78
W_D	2.19	2.20	2.15	2.03	2.02
$V(nA)$	47.43	47.02	46.57	45.11	44.82
W_v	1.92	1.92	1.92	1.83	1.83
W_D	2.15	2.12	2.05	1.95	1.92
Bechetti-Greenlees[d]					
V proton	55.16	55.54	55.89	56.60	56.75
W_v	3.24	3.24	3.24	3.24	3.24
W_D	7.37	7.43	7.52	7.74	7.77
$V(nB)$	49.69	49.56	49.22	47.97	47.57
W_v	0.0	0.0	0.0	0.0	0.0
W_D	7.29	7.49	7.52	7.52	7.55
$V(nA)$	46.80	46.59	46.50	46.38	46.31
W_v	0.0	0.0	0.0	0.0	0.0
W_D	7.48	7.42	7.33	7.36	7.33
V_1	15.0	16.0	17.0	20.0	21.0
W_1	12.0	12.0	12.0	12.0	12.0

[a]Out-going neutrons from the $(p,n)_{IAS}$ reaction.
[b]Neutrons elastically scattered from the target. The energies are those from measurements found in the literature.
[c]Menet *et al.* OMP (Ref. 31).
[d]Becchett-Greenlees OMP (Ref. 32).

in the proton global sets. (See Table II for the values of all the OM parameters used in the calculation.) The calculated differential cross sections from the (p,n) reaction to the isobaric analog levels of the g.s. and 137-keV levels are shown in Fig. 6. The measured analog cross sections are compared first with the calculated cross sections to the analog of ^{181}Ta ground state (upper curves); second, they are compared with the sum (lower curves) of the calculated cross sections for the analogs of the g.s. and 137-keV levels. The values of the real and imaginary parts of the isovector potential, V_1 and W_{D1}, in these calculations are 15 and 12 MeV, respectively, which were obtained from the best fit to the measurements. The calculated cross sections with the two different OMP sets are rather close, although Menet *et al.*[31] OMP (solid curves) give a slightly better fit to the data. With the exception of the forward angles, $\theta \leq 20°$, the calculated differential cross sections for the ground-state analog in ^{181}W are in good agreement with the data; the addition of the 137-keV analog level improves the fit at the forward angles at the expense of the larger angles, $\theta \geq 80°$, where the fit is worsened. Clearly, an overall better fit could have been obtained by searching on the parameters of the OMP. Specifically, the magnitude of the cross sections at large angles is quite sensitive to the depth and geometrical parameters of the isoscalar and isovector absorption potentials, W_0 and W_1. However, it was felt that the lack of proton scattering data did not warrant such a search since the values obtained would not have resulted from a simultaneous fit of the (p,p) and $(p,n)_{IAS}$ data in the spirit of the Lane model.

^{197}Au$(p,n)_{IAS}$ ^{197}Hg

The low-lying excited levels in ^{197}Au are described[16,17] by the coupling of the odd $d_{3/2}$ proton to the g.s. (0^+) and 2^+ excited states, respectively, of the ^{196}Pt core (core-excitation model). In the level scheme shown in Fig. 7, the levels marked with asterisks result from the coupling $J^\pi = |J_c, i, J^\pi$, where the odd nucleon in the state, $j = \frac{3}{2}^+$, is coupled to a core with angular momentum $J_c = 2^+$ to yield a total angular momentum J^π: $\frac{1}{2}^+$ (0.077-MeV level), $\frac{3}{2}^+$ (0.269-MeV level), $\frac{5}{2}^+$ (0.279-MeV level), and $\frac{7}{2}^+$ (0.548-MeV level). With the exception of the $\frac{7}{2}^+$ ($E_{exc} > \Delta E_{IAS}$), all these levels and their respective analogs in ^{197}Hg ($\Delta_C = -18.74$ MeV) are included in the CC calculations of the $(p,n)_{IAS}$ cross sections shown in Fig. 8. A weak coupling model has been assumed in the calculation of the deformation parameters for the excited levels with

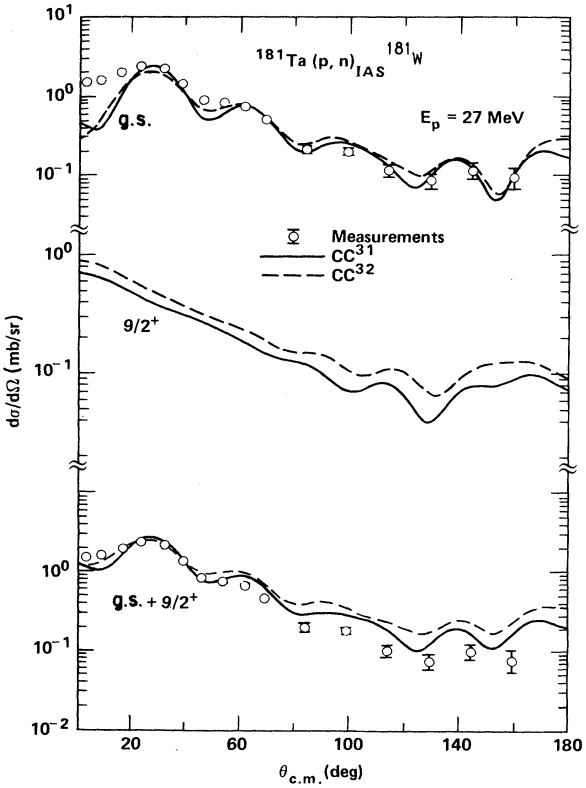

FIG. 6. Comparison of the measured $(p,n)_{IAS}$ differential cross sections for ^{181}Ta at 27 MeV with CC calculations using Lane-consistent OMP. The OM parameters are from Ref. 31 (solid curves) and Ref. 32 (dashed curves). The upper curves are the calculated g.s. analog cross sections; the lower curves result from the sum of the g.s. and the excited 0.136-MeV ($\frac{9}{2}^+$) analog cross sections.

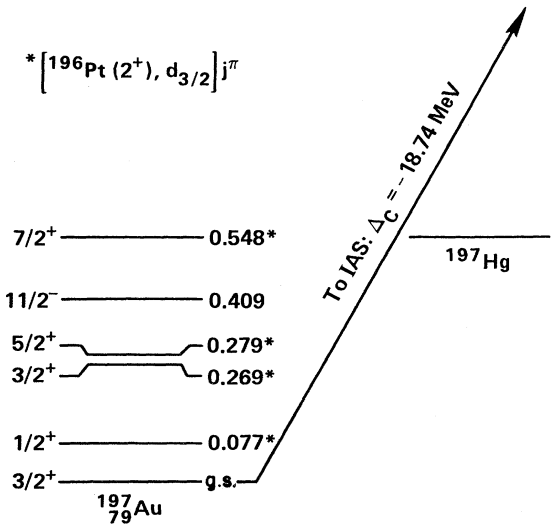

FIG. 7. Level scheme for the low-lying excited levels of ^{197}Au. The $\frac{1}{2}^+$, $\frac{3}{2}^+$, and $\frac{5}{2}^+$ excited levels and their analogs have been included in the CC calculations of the g.s. $(p,n)_{IAS}$ cross sections.

$$\beta(J_f)=\beta(J_c)\left[\frac{2J_f+1}{(2j+1)(2J_c+1)}\right]^{1/2}, \tag{7}$$

where $\beta(J_c)$ is the deformation parameter for the ^{196}Pt core. A value of $\beta_2=0.125$ taken from Ref. 36 was used in the calculations.

As in the ^{181}Ta calculations, no elastic proton differential cross sections at 27 MeV were available; accordingly, the proton and neutron OM parameters used in the CC calculations are those from the global sets,[31,32] where the proton and neutron potentials were calculated following the same procedure as in the Ta calculations (see Table II). For both sets, the best fits to the data were obtained with real and imaginary isovector strengths of 16 and 12 MeV, respectively, with the appropriate corrections made to the isoscalar strengths, V_0 and W_{D0}. On the left side of Fig. 8 are plotted the calculations for the (p,n) differential cross sections from the $\frac{1}{2}^+$, $\frac{3}{2}^+$, and $\frac{5}{2}^+$ excited analog states in ^{197}Hg. The solid curves have been calculted with Menet *et al.*[31] OM parameters, and the dashed ones with BG (Ref. 32) global parameters.

On the right side of Fig. 8 the measurements are compared with the calculations for the g.s. analog (upper curves) and with the sum of the calculations for the g.s., $\frac{1}{2}^+$, $\frac{3}{2}^+$, and $\frac{5}{2}^+$ analogs (lower curves). The contribution to the sum of the cross sections from the excited analog states is rather small; the magnitudes of the (p,n) cross sections for the $\frac{1}{2}^+$, $\frac{3}{2}^+$, and $\frac{5}{2}^+$ excited analogs are about 7%, 5%, and 3%, respectively, of the g.s. cross sections, which are about 5 mb for either set of OM parameters. The agreement between the calculations and measurements is fairly good for either OMP although the Menet *et al.*[31] OM parameters fit the backward angles somewhat better and BG (Ref. 32) fit the forward angles better. A third CC calculation, including only the g.s., $\frac{5}{2}^+$ level, and their respective analog levels, was carried out with BG parameters assuming a rotational description[37] for the low-lying level structure of ^{197}Au. The shape of the calculated (p,n) angular distributions and their sum was very close to those plotted in Fig. 8 for the same OM parameters, with slightly higher values for the cross sections at larger angles, $\theta \geq 120°$. Because the g.s. analog transition is the predominant contribution to the $(p,n)_{IAS}$ cross sections in both vibrational and rotational calculations, the measurements do not permit a choice between these two descriptions.

^{209}Bi(p,n)$_{IAS}$ ^{209}Po

The CC calculations carried out to describe the (p,n) reaction to the isobaric analog state of the ^{209}Bi ground state in ^{209}Po included only the g.s. and its analog ($\Delta_C=-19.31$ MeV). ^{209}Bi is well described by a weak coupling model,[19] where the g.s. results from the coupling of an $h_{9/2}$ proton to the ^{208}Pb 0^+ core, while the septuplet of levels around 2.6 MeV ($J^\pi=\frac{3}{2}^+,\ldots,\frac{15}{2}^+$) is described by the coupling of this $h_{9/2}$ proton to the 3^- collective level in ^{208}Pb. Since the excitation energies of these levels are much higher than the intrinsic width of the analog level ($\Delta E_{IAS}\simeq 300$ keV), they were not included in the CC

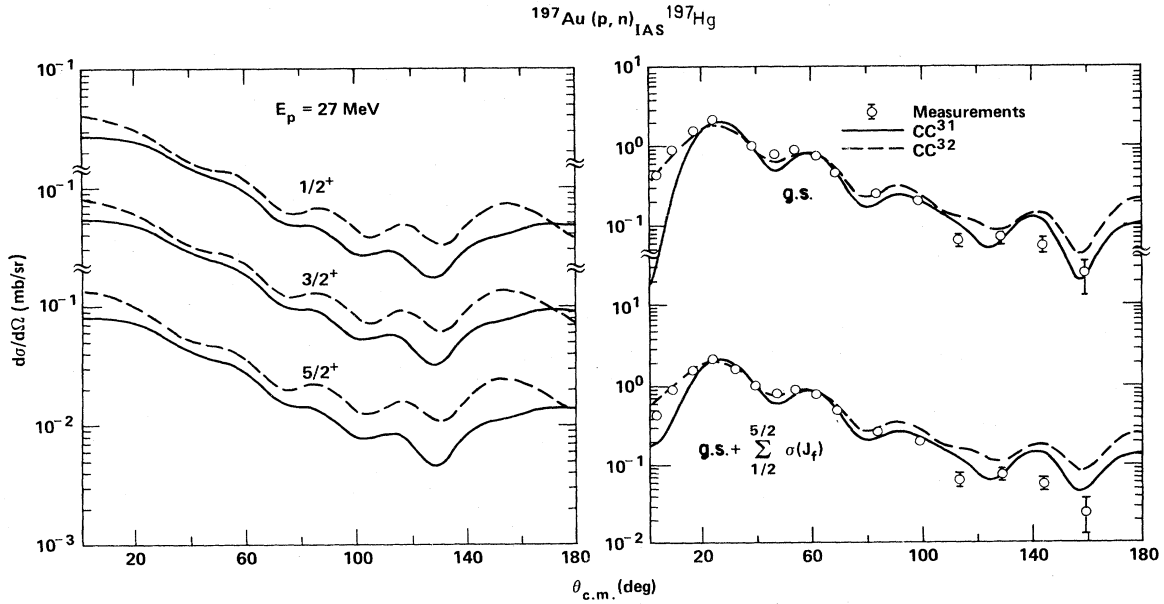

FIG. 8. Comparison of the measured $(p,n)_{IAS}$ differential cross sections for ^{197}Au at 27 MeV with CC calculations using Lane-consistent OMP. The OM parameters are from Ref. 31 (solid curves) and Ref. 32 (dash curves). The upper right side curves are the calculated g.s. analog cross sections; the lower curves correspond to the sum of the g.s. analog and excited analog cross sections for the 0.077-MeV ($\frac{1}{2}^+$), 0.269-MeV ($\frac{3}{2}^+$), and 0.279-MeV ($\frac{5}{2}^+$) levels. The calculated $(p,n)_{IAS}$ cross sections for the excited levels are shown on the left side.

calculations. These calculations using the Lane formalism is described earlier to calculate the OM parameters for the proton and neutron channels are shown in Fig. 9; solid curves were calculated with Menet *et al.*[31] OMP, and dashed curves were calculated with BG (Ref. 32) potentials. From best fits to the data, the values of the real and imaginary isovector potential were found to be 17 and 12 MeV, respectively. Because of limitations in the size of the CC code[35] and because of the large value of the ground- and analog-state spins, $\frac{9}{2}^-$, it was not possible to include in the CC calculations all the levels of the above septuplet. However, in order to study the effect of the coupling of the g.s. to the excited collective levels and their respective analog levels, a CC calculation was carried out where the ^{209}Bi g.s. assumed to be a 0^+, was coupled to a 3^- level at 2.6-MeV excitation and the corresponding analog states in ^{209}Po. All couplings between the four levels were included (assuming an $L=3$ angular momentum transfer between the proton channels in the target and neutron channels in the final nucleus). The magnitude of the octupole deformation parameters was $\beta_3(J_c)=0.125$ (Ref. 38). The calculated (p,n) differential cross sections using BG OM parameters are plotted in Fig. 9 (dash-dotted line). Minor changes in the slope of the angular distribution are observed as a result of these couplings without a clear improved fit to the measurements.

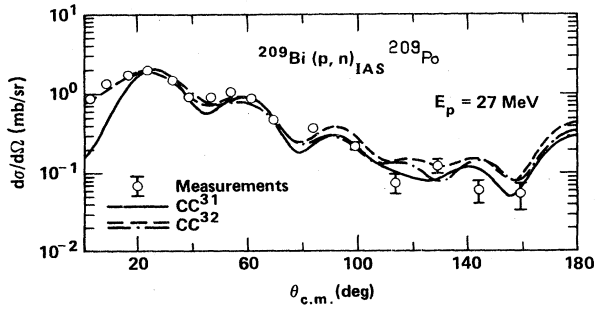

FIG. 9. CC fits to the measured $(p,n)_{IAS}$ differential cross sections for ^{209}Bi at 27 MeV using Lane-consistent OMP. The OM parameters are from Ref. 31 (solid curve) and from Ref. 32 (dash and dash-dotted curves). See text for details of the couplings used in these calculations.

ELASTIC NEUTRON DIFFERENTIAL CROSS-SECTION CALCULATIONS

The calculation of the (n,n_0) differential cross sections in the (nA) channel [Eq. (5)] is implicit in the CC calculations of the $(p,n)_{IAS}$ reaction, where the g.s. and inelastic levels in the target nucleus (proton channels) and their analog states in the final nucleus (neutron channels) are included.

The neutron OMP for neutrons elastically scattered from the target were obtained following the same calculational procedure described earlier for the neutrons scattered from the analog state [(nB) channel]. Starting from the adjusted proton global sets[31,32] (Table I), the Coulomb

correction term was dropped, and the neutron potentials were calculated at the neutron energy, E_n. The isovector potentials for the different targets were those obtained from the CC calculations carried out to fit the $(p,n)_{IAS}$ measurements.

CC calculations were carried out to obtain the elastic neutron differential cross sections using OMP prescribed by Eq. (5). The inelastic levels included in the $(p,n)_{IAS}$ calculations discussed above were also included in the calculations of the (n,n_0) cross sections. The calculated cross sections are compared with existing measurements[7–9] in Figs. 10 and 11. The results for the lighter nuclei, ^{181}Ta, ^{197}Au, and ^{209}Bi, are shown in Fig. 10, where the solid lines correspond to the calculations with the OM parameters obtained from the proton OMP given by BG global set[32] (Table II). The dashed curves have been calculated using neutron OMP from the Rapaport *et al.*[20] global set.

The overall agreement between the neutron elastic cross sections calculated with OMP extracted from the CC calculations to (p,n) and $(p,n)_{IAS}$ data is fairly good and consistently better than that obtained from Schery *et al.*[10] with OMP extracted from a DWBA calculation of the $(p,n)_{IAS}$ cross sections. It is interesting to point out that in a search of OM parameters, limited only to the values of the real and imaginary isovector strengths, the calculated (n,n) cross sections using the Lane formalism [Eqs. (3) and (5)] compare very well with calculations carried out with neutron global parameters optimized to fit neutron data, as is the case for the Rapaport *et al.* global set.

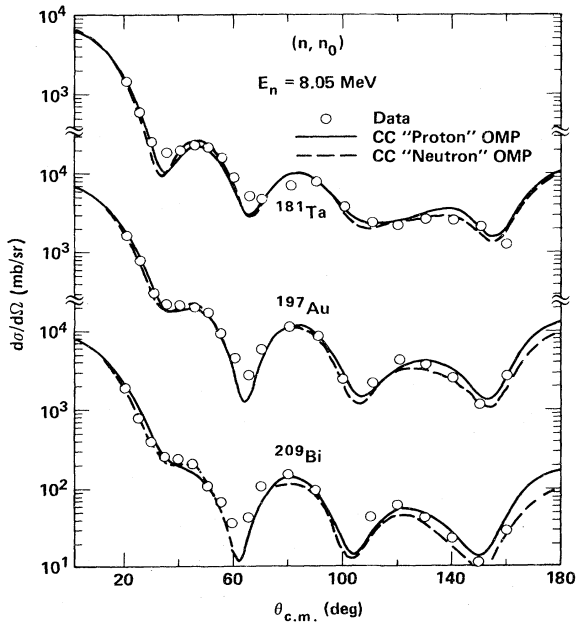

FIG. 10. CC calculations of the elastic neutron differential cross sections from ^{181}Ta, ^{197}Au, and ^{209}Bi at 8.05 MeV. The solid curves have been calculated with OM parameters obtained from the present Lane-consistent analysis of the respective (p,p_0) and $(p,n)_{IAS}$ cross sections, using the proton parameters from the global set of Ref. 32. The dashed curves have been obtained with neutron OM parameter from the global set of Ref. 20. The data are from Ref. 8.

The calculated elastic neutron cross sections for ^{232}Th and ^{238}U are compared in Fig. 11 (upper curves) with the measurements of Batchelor *et al.*[9] The OM parameters are derived from Menet *et al.*[31] proton OMP, which gave the best fit to proton scattering data[11] at 26 MeV. Shown for comparison (dashed lines) are calculations with the neutron potentials taken from Madland and Young[21] global set, where the parameters have been optimized for this region of the Periodic Table and energy range, 10 keV $\leq E_n \leq 10$ MeV. Because the measurements[9] did not resolve the low-lying excited 2^+ and 4^+ levels from the g.s. cross sections, the sum of the calculated differential cross sections for these three levels (lower curves) is also compared with the measurements, and good agreement is observed.

From the comparisons shown in Figs. 10 and 11, it may be concluded that the calculations with neutron potentials obtained from the analysis of the (p,p) and $(p,n)_{IAS}$ data, using global proton parameters, reproduce the (n,n) measurements as well as the calculations with optimum neutron potentials for these nuclei.

A criticism to the above analysis could be that a Coulomb correction was only made for the real potential and not for the imaginary ones. This apparent lack of consistency was a result simply of the way in which the proton potentials had been parametrized originally.[31,32] An alternative approach would be to make a "full" Coulomb correction for all potential terms, producing Lane model consistency, i.e., the isovector strengths are given by the difference of proton and neutron potentials. This can be done simply by taking the isoscalar and isovector potentials as previously determined at 27 MeV, substituting the values of Eq. (5), and equating the result to the neutron potential at a neutron energy of 27 MeV minus the Coulomb energy difference, which is close to the energy of the neutron scattering measurements. This was done for the case of ^{232}Th and the resulting calculation was compared to the data. The results were not significantly different from the previous calculation and the large errors on the neutron data did not allow a choice to be made between the two calculations. Consequently, this approach was not pursued further.

CONCLUSIONS

In the present work, we have presented our measurements of the $(p,n)_{IAS}$ charge-exchange cross sections for ^{181}Ta, ^{197}Au, ^{209}Bi, ^{232}Th, and ^{238}U at 27 MeV and ^{232}Th and ^{238}U at 26 MeV. The analysis of the data has been carried out with the Lane model using Tamura's coupled channel formalism. The Lane coupled equations for the system, proton + target→neutron + analog, were solved exactly, and both the $(p,n)_{IAS}$ data and (p,p) data, when available, were analyzed simultaneously.[11] Because of strong couplings between the low-lying excited levels to the g.s. and analog levels for the above nuclei, the description of the $(p,n)_{IAS}$ transitions must include these levels in the CC calculations. Furthermore, the inelastic levels had to be included in the solution of the Lane coupled equations, since the intrinsic width[12,13] of the analog state

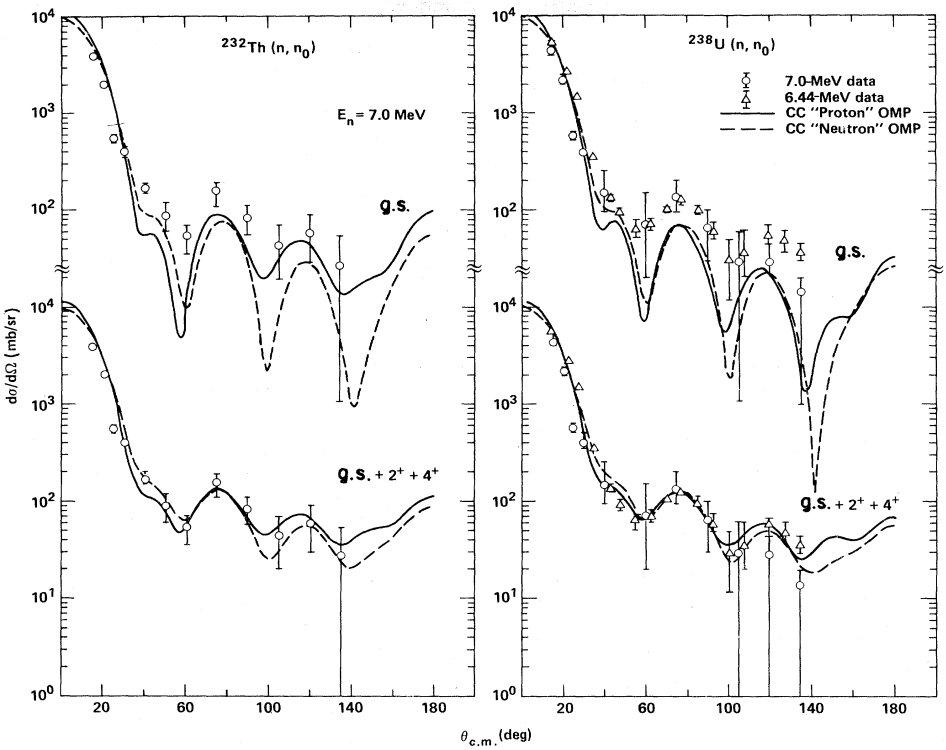

FIG. 11. CC calculations of the elastic neutron differential cross sections for ^{232}Th and ^{238}U at 7.0 MeV. The solid curves have been calculated with OM parameters obtained from the present Lane-consistent analysis of the respective (p,p_0) and $(p,n)_{IAS}$ cross sections using the proton parameters from the global set of Ref. 31. The dashed curves have been obtained with neutron OM parameters optimized for the actinide region (Ref. 21). The data are from Ref. 9.

($\geq$200 keV) for the nuclei studied here does not permit a separation of the g.s. analog from the excited analog levels with excitation energies less than the width of the analog state.

The OMP for the proton and neutron channels were extracted from the global proton sets of Menet *et al.*[31] and Becchetti and Greenlees[32] following the Lane formalism. The values of the real and imaginary isovector potentials, V_1 and W_1, were obtained from the best fit to the $(p,n)_{IAS}$ differential cross sections. The values of V_1 increased approximately as $A^{1/3}$ between ^{181}Ta ($V_1=15$ MeV) and ^{238}U ($V_1=21$ MeV) for the same values of the geometrical parameters prescribed by the global sets and an isovector absorption potential $W_1=12$ MeV. This relation cannot be taken very seriously, however, since no extended search for other values of the absorption potential was carried out. Other than the isovector strengths, V_1 and W_1, no search of optical parameters was carried out for the fits obtained for the $(p,n)_{IAS}$ measurements and (n,n) data.[7–9] The strengths of the real and imaginary isoscalar potentials, when used to solve the CC equations in the proton and neutron channels, were corrected appropriately for the values of V_1 and W_1 in order to preserve the total strength of the nuclear potential given by the global sets.[31,32] Both global OMP gave comparable fits to the measured $(p,n)_{IAS}$ differential cross sections for the lighter nuclei, ^{181}Ta, ^{197}Au, and ^{209}Bi, with the BG (Ref. 32) set yielding better fits for the neutron elastic data. For ^{232}Th and ^{238}U, Menet *et al.*[31] OMP gave an overall better fit to the (p,p), $(p,n)_{IAS}$, and (n,n) differential cross sections.

The elastic neutron angular distributions calculated with the OMP extracted from the present Lane CC calculations agree very well with the available measurements between 7 and 8 MeV. The quality of these fits is comparable to those obtained using calculations carried out with neutron global paremeters[20,21] optimized to fit the existing neutron data. The poorer agreement[10] obtained with neutron OMP extracted from DWBA calculations shows the inadequacy of the latter for nuclei where collective effects are important.

In summary, we conclude that the Lane formalism generalized to include channel coupling effects is a powerful tool that can be used to predict neutron inelastic cross sections for heavy nuclei, including the actinide region, as successfully as has been done for lighter nuclei.[2–4] The quality of the agreement between the calculations and the measurements depends on making use of coupled-channel techniques in the calculational analysis of the proton elastic and charge exchange measurements and by the completeness of the physical picture of the interaction when collective effects are important such as for the deformed nuclei Ta, Th, and U.

ACKNOWLEDGMENTS

The authors would like to thank Professor V. A. Madsen for stimulating discussions and a critical reading of the manuscript. This work was performed under the auspices of the U.S. Department of Energy by Lawrence Livermore National Laboratory under Contract No. W-7405-Eng-48.

---

*Present address: Department of Physics, Ohio University, Athens, OH 45701.

[1]A. M. Lane, Phys. Rev. Lett. 8, 171 (1962); Nucl. Phys. 35, 676 (1962).

[2]J. D. Carlson, C. D. Zafiratos, and D. A. Lind, Nucl. Phys. A249, 29 (1975).

[3]D. M. Patterson, R. R. Doering, and A. Galonsky, Nucl. Phys. A263, 261 (1976).

[4]D. H. Fitzgerald, G. W. Greenlees, J. S. Lilley, C. H. Poppe, S. M. Grimes, and C. Wong, Phys. Rev. C 16, 2181 (1977).

[5]L. F. Hansen and M. L. Stelts, Phys. Rev. 132, 1123 (1963).

[6]L. F. Hansen, M. L. Stelts, and J. J. Wesolowski, Phys. Rev. 143, 800 (1966).

[7]J. R. Beyster, M. Walt, and E. W. Salmi, Phys. Rev. 104, 1319 (1956).

[8]B. Holmquist and T. Wiedling, Nucl. Phys. A150, 105 (1970); A188, 24 (1972).

[9]R. Batchelor, W. B. Gilboy, and J. H. Towle, Nucl. Phys. A65, 236 (1965).

[10]S. D. Schery, D. A. Lind, H. W. Fielding, and C. D. Zafiratos, Nucl. Phys. A234, 109 (1974).

[11]L. F. Hansen, I. D. Proctor, D. W. Heikkinen, and V. A. Madsen, Phys. Rev. C 25, 189 (1982).

[12]A. M. Lane and J. M. Soper, Nucl. Phys. 37, 663 (1969).

[13]C. D. Kavaloski, J. S. Lilley, P. Richard, and N. Stein, Phys. Rev. Lett. 16, 807 (1966); G. M. Crawley, P. S. Miller, A. Galonsky, T. Amos, and R. Doering, Phys. Rev. C 6, 1890 (1972).

[14]A. Bohr and B. R. Mottelson, K. Dan. Vidensk. Selsk. Mat.-Fys. Medd. 27, No. 16 (1953), Series I.

[15]B. R. Mottelson and S. G. Nilsson, K. Dan. Vidensk. Selsk. Mat.-Fys. Medd. 1, No. 8 (1959), Series II.

[16]A. Braunstein and A. De-Shalit, Phys. Lett. 1, 264 (1962).

[17]R. P. Sharma, Nucl. Phys. A154, 312 (1970).

[18]F. K. McGowan, W. T. Milner, R. L. Robinson, and P. H. Stelson, Ann. Phys. (N.Y.) 63, 549 (1971).

[19]K. Arita and H. Horie, Phys. Lett. 30B, 14 (1969).

[20]J. Rapaport, V. Kulkarni, and R. W. Finlay, Nucl. Phys. A330, 15 (1979). (See other references in this paper.)

[21]D. G. Madland and P. G. Young, in *Proceedings of the Conference on Neutron Physics and Nuclear Data, Harwell, England, 1979,* edited by C. Kousnetzoff (NEA-AEN, Paris, 1978), pp. 349—354.

[22](a) J. C. Davis, J. D. Anderson, E. K. Freytag, and D. R. Rawles, IEEE Trans. Nucl. Sci. 20, 213 (1973). (b) C. Wong, S. M. Grimes, C. H. Poppe, V. R. Brown, and V. A. Madsen, Phys. Rev. C 26, 889 (1982).

[23]A. Galonsky, G. M. Crawley, P. S. Miller, R. R. Doering, and D. M. Patterson, Phys. Rev. C 12, 1072 (1975).

[24]T. N. Taddeucci, J. Rapaport, D. E. Bainum, C. D. Goodman, C. C. Foster, C. Gaarde, J. Larsen, C. A. Goulding, D. J. Horen, T. G. Masterson, and E. Sugarbaker, Phys. Rev. C 25, 1094 (1981).

[25]D. J. Horen, C. D. Goodman, C. C. Foster, C. A. Goulding, M. B. Greenfield, J. Rapaport, D. E. Bainum, E. Sugarbaker, T. G. Masterson, and F. Petrovich, Phys. Lett. 95B, 27 (1980).

[26]H. W. Fielding, S. D. Schery, D. A. Lind, and C. D. Zafiratos, Phys. Rev. C 10, 1560 (1974).

[27]J. D. Anderson, C. Wong, and J. W. McClure, Phys. Rev. 138, B615 (1965).

[28]J. P. Jeukenne, A. Lejeune, and C. Mahaux, Phys. Rev. C 15, 80 (1977).

[29]G. R. Satchler, in *Isospin in Nuclear Physics,* edited by D. H. Wilkinson (North-Holland, Amsterdam, 1969).

[30]J. Rapaport, Phys. Lett. 92B, 233 (1980).

[31]J. J. Menet, E. E. Gross, J. J. Malanify, and A. Tucker, Phys. Rev. C 4, 1114 (1971).

[32]F. D. Becchetti and G. W. Greenlees, Phys. Rev. 182, 1190 (1969).

[33]V. A. Madsen and V. R. Brown, in *The (p,n) Reaction and the Nucleon-Nucleon Force,* edited by C. D. Goodman, S. M. Austin, S. D. Bloom, J. Rapaport, and G. R. Satchler (Plenum, New York, 1980), p. 409.

[34]T. Tamura, Rev. Mod. Phys. 37, 679 (1965).

[35]M. J. Stomp, F. A. Schmittroth, and V. A. Madsen, USAEC Technical Report, Contract No. At(45-1)-222, 1972 (unpublished).

[36]P. H. Stelson and L. Grodzins, Nucl. Data Sect. A 1, 21 (1965).

[37]K. G. Prasad, R. P. Sharma, and B. V. Thosav, in *Proceedings of the International Conference on Nuclear Stucture, Montreal, Canada, 1969,* edited by D. A. Bromley and E. W. Vogt (North-Holland, Amsterdam, 1960).

[38]M. J. Martin, Nucl. Data Sheets 2, 545 (1977).